Structures and Charging of α-Alumina (0001)/Water Interfaces Studied by Sum-Frequency Vibrational Spectroscopy

Luning Zhang,[†] Chuanshan Tian,[†] Glenn A. Waychunas,[‡] and Y. Ron Shen,[†]*

Department of Physics, University of California, Berkeley, CA 94720, and Earth Sciences Division, Lawrence Berkeley National Laboratory, Berkeley, CA 94720

Abstract: Sum-frequency vibrational spectroscopy in the OH stretch region was employed to study structures of water/α-Al_2O_3 (0001) interfaces at different pH values. Observed spectra indicate that protonation and deprotonation of the alumina surface dominate at low and high pH, respectively, with the interface positively and negatively charged accordingly. The point of zero charge (p.z.c.) appears at pH ~6.3, which is close to the values obtained from streaming potential and second harmonic generation studies. It is significantly lower than the p.z.c. of alumina powder. The result can be understood from the pK values of protonation and deprotonation at the water/α-Al_2O_3 (0001) interface. The p.z.c. of amorphous alumina was found to be similar to that of powder alumina.

* Corresponding author. E-mail: yrshen@berkeley.edu. Fax (510) 643 8923.

† University of California.

‡ Lawrence Berkeley National Laboratory.

Introduction

In water, a metal oxide surface terminated with hydroxyl groups can be protonated or deprotonated, leaving the surface with a net positive or negative charge. In both natural and industrial environments, many chemical reactions can be initiated on such oxide surfaces and they are unavoidably affected by the charging properties of the surface.[1-3] Processes involving sorption process,[1] soil and aquifer chemical reactions,[4] production and stabilization of colloidal systems[5] heterogeneous catalysis,[6] and nanoparticle phase stability[7] are just a few examples. It is fundamentally important to know how the microscopic surface structure of an oxide controls the surface charging behavior and affects the interfacial water structure.

In this paper, we report the use of sum-frequency vibrational spectroscopy (SFVS) to study water/α-Al_2O_3 (0001) interface and its charging behavior in response to pH variation of the contacting aqueous solution. Single crystals of α-Al_2O_3, known as sapphire or corundum, are important in industrial applications and serves as an excellent model system for studies of water/oxide interfaces. It is anhydrous and its edge-sharing AlO_6 octahedral structure is seen in many other minerals, especially the mica group. Hence the study of corundum is an important first step in understanding water interactions with such types of layers. Being a relatively inert mineral, α-Al_2O_3 can maintain high-quality crystalline surfaces for extended periods even under relatively harsh conditions.[8,9] There have been studies on α-Al_2O_3 that provide information on geometries of adsorption sites[10,11] and surface structures.[12] In particular, the charging behavior of alumina surfaces, especially the point of zero charge (p.z.c.), which is a fundamental property of water/oxide interfaces, has sparked interests of scientists for more than half a century.[13-15]

Previous studies on p.z.c. of alumina fall into two categories: the first one utilizing streaming potential,[16,17] electrophoretic mobility,[18] and potentiometric titration[19] to probe surface charge density directly, and the second one using atomic force microscopy (AFM) in the force-distance operation mode,[17,20] second harmonic generation (SHG),[21-22] and SFVS[23] to probe surface interaction and ordering of interfacial molecular species affected by charging behavior. Kosmulski has written excellent reviews

on studies of alumina crystalline powders.[13,24-26] The p.z.c. of crystalline powders was found to be between pH 8 and 10. For studies of single-crystal alumina surfaces, only streaming potential, AFM, SHG and SFVS have been used. Except for one of the earlier reports on sapphire/water interface,[23] all recent studies found p.z.c. of α-Al_2O_3 (A, R, and C-planes) to be around pH5-6. This difference of nearly three pH units between single crystals and crystalline powders is surprising. Based on the results of an SHG study, Stack et al. proposed that this discrepancy might arise from a gibbsite-like surface structure.[21] Franks and Meagher suggested that the high p.z.c. found for powder samples could be due to surface hydroxyls bound to only one aluminum atom underneath.[17] Kershner et al. provided concrete results showing that the higher p.z.c. of powders comes from the multiple facets of crystalline particles in the powder.[16] A recent SHG study by Eisenthal's group suggested that the p.z.c. difference might be due to higher defect density on Al-(hydro)oxide particles.[22] These results all indicate that the differences in O-Al coordination at the surface could be responsible for the large disparity of p.z.c. values observed. Clearly a more thorough understanding of the charging behavior of alumina surfaces and the corresponding molecular-level surface structure is needed.

SFVS is a unique probe for vibrational spectra of liquid/solid interfaces.[27-29] We have used it to obtain vibrational spectra of water/α-Al_2O_3(0001) interface in the OH stretch region with different bulk solution pH values. Similar to those of other water interfaces, each spectrum generally exhibits a dangling OH peak at ~3700 cm^{-1}, and a liquid-like and an ice-like band at ~3450 cm^{-1} and ~3200 cm^{-1}, respectively. Yeganeh et al.[23] first employed SFVS to probe OH stretch vibrations of water/alumina interfaces for hydrate and dehydrated alumina surfaces. They used a sample with unspecified crystal plane and also surface treatments different from the common ones. They obtained spectra different from ours, including both the absence of the 3700 cm^{-1} peak and a p.z.c. different from previous studies on single crystal alumina. In our SFVS spectra, the amplitudes of the liquid-like and ice-like bands, which can be positive or negative, reflecting the net polar orientation of the contributing water species, changes with pH. The spectra indicate that the water interfacial structure is a highly distorted ice-like hydrogen-bonding network, with the first layer of adsorbed molecules hydrogen-bonded to O or H at the surface

sites. In this study, we found that the signs of the resonant amplitudes signify the net polar orientations of interfacial water species contributing to the resonances. In particular, we notice that for the case of the water/α-Al_2O_3 (0001) interface, the strength of the ice-like band can be a qualitative measure of the surface charges (degree of protonation or deprotonation) and the sign of its amplitude denotes the sign of the surface charges.

In addition, our SFVS results with different pH values allow us to monitor when protonation or deprotonation dominates at the surface, and accordingly yield an estimation of the p.z.c.. We find that the p.z.c. for α-Al_2O_3(0001) occurs at pH ~ 6.3, in agreement with the values found in earlier studies, especially those from SHG measurements.[16,22] The difference between SFVS and SHG is that the former provides a great deal of microscopic structural information through the interfacial vigrational spectra. We can understand from the SFVS results how the p.z.c. is related to the reaction constants of protonation and deprotonation at a surface, and can explain why the p.z.c. of α-Al_2O_3 (0001) is significantly lower than that of powder alumina. We also used SFVS to obtain the p.z.c. of the water/amorphous alumina interface, and found it was close to that of crystalline powder, confirming the suggestion that the two have similar average microscopic surface structure.[16,17,22]

The paper is structured as follows: Sections 2 and 3 describe briefly the theoretical background for SFVS and experimental arrangement for the work. Section 4 presents the spectroscopic results and analysis, followed by discussion of the results in Section 5. A brief conclusion is given in Section 6.

Theoretical Background of SFVS

The theoretical background of SFG has been described in several reviews.[30-34] The SF signal generated by overlapping a visible input with intensity I_1 and fixed frequency ω_1 and an IR input with intensity I_2 and tunable frequency ω_2 at an interface is given by:

$$S(\omega = \omega_1 + \omega_2) \propto \left| [\vec{L}(\omega) \cdot \hat{e}] \cdot \vec{\chi}_S^{(2)} : [\hat{e}_1 \cdot \vec{L}(\omega_1)][\hat{e}_2 \cdot \vec{L}(\omega_2)] \right|^2 I_1 I_2 \qquad (1)$$

where $\hat{e}_i$ and $\vec{\vec{L}}(\omega_i)$ denote, respectively, the unit polarization vector and the tensorial Fresnel transmission coefficient of the surface at ω_i, and $\vec{\vec{\chi}}_S^{(2)}$ is the surface nonlinear susceptibility tensor that can be expressed, for discrete resonances, by

$$\vec{\vec{\chi}}_S^{(2)} = \vec{\vec{\chi}}_{NR}^{(2)} + \sum_q \frac{\vec{\vec{A}}_q}{\omega_{IR} - \omega_q + i\Gamma_q} \qquad (2a)$$

and for continuum resonances, by

$$\vec{\vec{\chi}}_S^{(2)} = \vec{\vec{\chi}}_{NR}^{(2)} + \int \frac{\vec{\vec{A}}_q \rho(\omega_q)}{\omega_{IR} - \omega_q + i\Gamma_q} d\omega_q \qquad (2b)$$

In the above equations, $\vec{\vec{\chi}}_{NR}^{(2)}$ describes the nonresonant contribution, $\vec{\vec{A}}_q$, ω_q, and Γ_q represent the amplitude, frequency, and damping constant of the qth vibrational resonance, respectively, and $\rho(\omega_q)$ is the density of modes at ω_q. Equation (2a) has been widely used to describe resonances in SF spectra. However, for water interfaces, it has been recognized that the OH stretch spectra come from interfacial water molecules with a wide variation of hydrogen-bonding geometry and strength and therefore are composed of a continuum of OH stretch resonances.[35,36] Thus Eq.(2b) is the more appropriate description of the SF response. Nevertheless, it is possible to approximate the interfacial response of water by Eq.(2a) with three resonances, one ice-like, one liquid-like, and one dangling OH, although one must have the correct signs of $\vec{\vec{A}}_q$. This is the approach we shall take in analyzing the SF spectra to be described later. Through fitting of an observed spectrum by Eq. (2a), we can deduce $\vec{\vec{A}}_q$, ω_q, and Γ_q for the qth resonance and also obtain the corresponding Im $\vec{\vec{\chi}}_S^{(2)}$ spectrum of the resonance. This deduced Im $\vec{\vec{\chi}}_S^{(2)}$ can be compared with experimentally obtained Im $\vec{\vec{\chi}}_S^{(2)}$ from phase measurement.

The amplitude $A_{q,ijk}$ of $\vec{\vec{\chi}}_S^{(2)}$ in the lab coordinates (x,y,z) is related to its counterpart $a_{q,lmn}^{(2)}$ of the molecular hyperpolarizability $\vec{\vec{\alpha}}_q^{(2)}$ in the molecular coordinates (ξ, η, ζ) through a coordinate transformation and an average over the molecular orientational distribution $f(\Omega)$:

$$A_{q,ijk} = N_S \int \sum_{l,m,n} \alpha_{q,lmn} (\hat{i} \cdot \hat{l})(\hat{j} \cdot \hat{m})(\hat{k} \cdot \hat{n}) f(\Omega) d\Omega \qquad (3)$$

The ratios of various $A_{q,ijk}$ can provide information on the average orientation of the molecular moiety contributing to the qth vibrational mode through Eq. (3).

An oxide surface in water can be protonated or deprotonated depending on the bulk pH. The resulting surface charges (and hence the surface field) and the preferred hydrogen-bonding geometry to the protonated or deprotonated surface sites, can reorient water molecules at the interface. This leads to an additional contribution to $\vec{\chi}_S^{(2)}$, which can now be written as[37-39]

$$\vec{\chi}_S^{(2)} = \vec{\chi}_{S0}^{(2)} + \Delta\vec{\chi}_S^{(2)} \qquad (4)$$

where $\Delta\vec{\chi}_S^{(2)}$ depends on the overall protonation or deprotonation. At the point of zero charge (p.z.c.), there is no protonation or deprotonation at the surface on average so that the surface field vanishes and $\Delta\vec{\chi}_S^{(2)} = 0$, which we can use as a criterion to find the p.z.c..

Experimental Arrangement

The epi-polished single-crystal α-Al_2O_3 (0001) samples of 5mm thickness were obtained from Princeton Scientific Corporation. Their chemical-mechanically polished surfaces had an root-mean-square roughness on the order of 0.2 nm. Before each experiment, the sample was cleaned in a sonication bath using the series of acetone, methanol and pure water for 10, 10, and 60 minutes, respectively. It was then mildly etched by 10-15mM solution of HNO_3 under sonication for 30 minutes followed by rinsing thoroughly with deionized water (resistivity: 18.3 MΩ·cm). The alumina sample was then blow-dried by filtered nitrogen gas. This procedure was used by other groups and is known to produce reliable results.[12,17,22] We used Telfon beakers for cleaning and etching, and a Teflon cell for measurement. Contact of alumina samples with glassware was avoided to ensure that no silicate contamination would be introduced.

As a sample for comparison, an amorphous alumina film of about 10 nm thick was prepared by the atomic layer deposition (ALD)[40] method on an α-Al_2O_3 (0001) substrate using tri-methyl aluminum and water reagents with N_2 as carrying gas. The amorphous film was then cleaned in organic solvents as described above. The SF spectrum of the film showed weak traces of CH stretch modes, indicating that there were minor organic contaminants left on the surface, presumably from the ALD process. The spectral intensity, in comparison with that of a monolayer of octadecanetrichlorosilane (OTS), indicates that the surface density of the residual -CH_3 contaminant is less than 1/nm^2.

The solution pH was adjusted by dissolving sodium hydroxide (99.998% pellets, Sigma-Aldrich) or hydrochloric acid (37%wt water solution, 99.999%, Sigma-Aldrich) in deionized water (resistivity 18.3MΩ·cm, Barnstead, Easypure RF). The solution pH was measured by a Beckmann pH meter equipped with an AccuTupH double-junction electrode. Solution with specific electrolyte concentration was prepared with the volumetric method by dissolving sodium chloride (>99.5%, ReagentPlus, Sigma) in a certain volume of water in a Teflon beaker.

Our SFVS setup has been described elsewhere.[27,28] A picosecond Nd:YAG laser with an optical parametric system was used to generate visible pulses at 532 nm and infrared pulses tunable between 2.6 and 3.7 μm, both having a pulse width of ~20 ps. The 532nm and IR pulses overlapped at the interface to be investigated with incident angles of 45° and 57°, respectively.The generated SF signal in the reflected direction was collected by a photomultiplier tube/gate integrator system. The signal was normalized against that from a z-cut α-quartz crystal. The phase measurement of $\vec{\chi}_S^{(2)}$ was performed using the phase-sensitive SF spectroscopic technique recently developed.[41] We have also used phase-sensitive sum-frequency spectroscopy[27,28] to determine the absolute orientation of the OH groups. The susceptibility $\chi^{(2)}$ is generally a complex value. In the intensity spectrum, which represents $|\chi^{(2)}|^2$, the phase information is missing. Only when we know both amplitude and phase, or the real and imaginary parts, of $\chi^{(2)}$, shall we be able to deduce information on the absolute orientation.[28,41]

Results

α-Al_2O_3 (0001)/air interface

We first obtained first the SF spectrum in the OH stretch region for the α-Al_2O_3 (0001) surface exposed only to air after cleaning and etching. As shown in Figure 1a, the main features in the spectrum are a strong peak at ~3700 cm^{-1} and a relatively weak and broad band at ~3430 cm^{-1}. The OH spectrum disappeared when the sample was dipped in deuterated water (D_2O), but reappeared after being dried and exposed in humid air (60% relative humidity) for a few hours (shown in Figure 1b). Heating of the sample to 600°C for one hour reduced the strength of the band at 3430 cm^{-1} by 60% but not that of the peak at 3700cm^{-1} except for an increase in its width. These results suggest that the spectrum came from hydroxyls at the alumina/air interface. The 3430 cm^{-1} band could originate from bonded OH stretches of adsorbed water species.[42] However, a MD simulation suggests that it could come from surface hydrogen-bonded OH groups.[43] As we shall discuss later, the 3700 cm^{-1} peak should come from Al_2OH groups with Al octahedrally bonded and OH protruding at the (0001) surface.[44-46] Electron energy loss spectroscopy has also provided evidence that this peak corresponds to hydroxlyated Al_2O groups.[47,48] The SF phase measurement found that the amplitudes ($\vec{\vec{A}}_q$) of both the 3430 cm^{-1} band and the 3700 cm^{-1} peak were negative, corresponding to O-H pointing away from the bulk alumina.

In Figure 2, the spectra of different polarization combinations, SSP (denoting S-, S-, and P-polarization for SF output, visible input, and infrared input, respectively), SPS and PPP, from the α-Al_2O_3(0001)/air interface are shown. The much weaker 3700 cm^{-1} peaks in SPS and PPP indicate that the protruding OH is oriented more along the surface normal. Fitting of the peaks using Eq.(2a) gave the amplitude ratio $A_{q,eff}$(SSP): $A_{q,eff}$(PPP): $A_{q,eff}$(SPS) = 1: 0.42 ±0.03: 0.06 ±0.03 for the peak. From Eq. (3) with the assumption that the orientational distribution f(Ω) is a delta function, we found that the tilt angle of dangling OH bond is around 26±2° with respect to the surface normal. This value is close to the expected tilted angle (~30°) of OH on a hydroxylated bulk-terminated α-Al_2O_3(0001) surface.

Water/α-Al_2O_3 interfaces

Figure 3 displays a set of SF-SSP spectra in the OH stretch range for the water/α-Al_2O_3 (0001) interface at different solution pH values. Spectra with different input/output polarizations, SSP, SPS, and PPP, are presented in Figure 4 for three different pHs. The 3700 cm^{-1} peak is still prominent. Compared to that of the air/α-Al_2O_3 (0001) interface, the peak intensity increased and the peak width narrowed. However, fitting of the 3700 cm^{-1} peaks indicates the strength to be nearly constant until pH reaches ~8.2, above which the strength decreases. Phase measurements show that the protruding OH contributing to this peak point away from the alumina substrate at all pH values. The polarization dependence of the peak (Figure 4) appears nearly the same as that for the air/alumina interface (Figure 2), indicating similar orientation for the protruding OH at the air/alumina and water/alumina interfaces. In the bonded OH stretch region of 3100 to 3600 cm^{-1} region, each spectrum can be decomposed into two bands, one centered at 3200 cm^{-1} (ice-like), and one centered at 3450 cm^{-1} (liquid-like). Their strengths vary appreciably with changes of pH. Both decrease with increase of pH until around pH 5.2. Between pH 5.2 and 7.4, the ice-like band has negligible strength and the liquid-like band remains almost unchanged. Above pH 7.4, the strengths of both bands increase with increase of pH. Phase measurements allowed us to deduce the $\mathrm{Im}\,\chi_S^{(2)}$ spectrum (shown in Figure 5 are representative data points at selected IR frequencies). The results indicated that the amplitudes of the two bands are both negative (same sign as the dangling OH at 3700 cm^{-1}) for pH < 5.2, but the amplitude of the ice-like band becomes positive when pH > 7.4. Plotted in Figure 6 are the amplitudes of the two bands deduced from fitting of the spectra versus pH. The sign of resonant amplitude describes the net polar orientation of the contributing OH species, and switching of the sign indicates switching of the net polar orientation. As we shall discuss later, this would happen close to the point of zero charge (p.z.c.) if $|\vec{\chi}_{S0}^{(2)}| << |\Delta\vec{\chi}_S^{(2)}|$, and we expect p.z.c. lies in the range of pH 5.2-7.4.

Discussion

Judging from the frequency, we can attribute the ~3700 cm^{-1} peak in the SF spectra to the stretch vibration of dangling OH at the alumina surface. Its existence at the air/alumina interface suggests that it is from $(Al)_nOH$ with H passivating the oxide surface. We assume the surface of α-Al_2O_3 (0001) with adsorbed H has a bulk-terminated structure depicted in Figure 7.[22,49] (A recent X-ray diffraction study found that the α-Al_2O_3 (0001) surface structure is relaxed mainly in the interlayer distance.[12] This would not seriously affect our discussion.) It shows the appearance of $(Al)_2OH$ groups at the surface with OH pointing out of the surface. The surface is hydrophilic as water molecules can still be hydrogen bonded to O at the surface. The H atoms of the dangling OH, however, must be so strongly bonded that they are not likely to participate in H-bonding with adsorbed water molecules and are also not easily deprotonated. Thus, when the surface is immersed in water, the dangling OHs are hardly affected; both the strength of the stretch vibration and the bond orientation should remain basically unchanged. This is very different from the silica case. When immersed in water, the H-passivated silica surface is readily deprotonated even at low pH (pH> 2).[27,28,50,51] Surface stresses in the alumina crystal could be relaxed in contact with bulk water. This would explain the observed narrowing of the dangling OH peak. At sufficiently large pH (> 8.2), deprotonation finally should set in, and accordingly the peak should reduce in strength. The above picture is consistent with our spectroscopic observations on the 3700 cm^{-1} peak described in Sec. 4. Isotope exchange of H and D at the surface must readily occur because OHs are exposed; strong bonding between H and O is evident from the fact that desorbing H is difficult even at high temperature (>600 °C).

The ice-like and liquid-like bands at 3200 and 3450 cm^{-1} in the $|\chi^{(2)}|^2$ spectra of water/alumina interfaces are similar to those observed at other water interfaces, but the resonant amplitudes A_q can have different signs for different interfaces reflecting different net polar orientations of contributing water species. Here, we assume that when the alumina surface is immersed in water, the originally adsorbed water molecules at the surface are rearranged and integrated into the H-bonding network of the interfacial water molecules. Variation of bulk pH in water can lead to protonation or deprotonation of

the alumina surface, and subsequently affect orientations of water species through the surface field produced by the surface charges as well as H-bonding of water molecules to the protonated or deprotonated alumina surface sites. For the α-Al_2O_3(0001) surface with $(Al)_2OH$ groups at the surface, it can be protonated (positively charged) at sufficiently low pH by the reaction $(Al)_2OH + H^+ \rightarrow (Al)_2OH_2^+$. The surface field created by the positive surface charges tends to reorient interfacial water molecules with O toward the surface. Hydrogen bonding of water molecules to the protonated sites also prefers to have O of the molecules point toward the surface. The situation is just the opposite when deprotonation sets in at sufficiently high pH by the reaction $(Al)_2OH + OH^- \rightarrow (Al)_2O^- + H_2O$. Both H-bonding to the deprotonated sites and surface field created by the negative surface charges tend to reorient the interfacial water molecules with H toward the surface.

To explain the observed spectral variation of the water/alumina interface with pH (Figures 3, 5, and 6), we consider first the case of a neutral alumina surface. As we mentioned earlier, interfacial water molecules should H-bond to $(Al)_2OH$ at the surface with their O attached to the –OH groups of the alumina surface. Such adsorbed molecules, however, are not likely to have a symmetric ice-like H-bonding geometry to the surface and to neighboring water molecules. Their OH stretches do not contribute to the ice-like band. They are the dominating contributors to the liquid-like band in the spectrum because surface-specific SFVS heavily favors molecules in the first adsorbed monolayer at the interface. (Water molecules away from the interface are rapidly disordered in both orientation and arrangement, and do not contribute much to the SF spectrum.) Their bonding geometry with O→H pointing toward the liquid makes A_q of the liquid-like band negative, same as the dangling OH peak at ~3700cm^{-1}. On the other hand, the ice-like band comes from water molecules next to the first monolayer with ice-like symmetric H-bonding to neighbors, and is expected to be very weak if the molecules have no preferred polar orientation as in the case of a neutral surface. As seen from Figure 6, this happens for pH in the range between 5 and 7.5. The pH value for zero surface charge is defined as the p.z.c.. From our result, we can set the p.z.c. for α-Al_2O_3 (0001) in aqueous solution at pH=6.3±1.2. We will have more discussion on this p.z.c. value later.

Figures 5 and 6 show that decreasing pH below 5 leads to a liquid-like band with increasingly negative amplitude and the appearance of the ice-like band also with increasingly negative amplitude. The increasingly negative amplitudes mean more water molecules oriented with O facing the surface. This can be understood by knowing that the alumina surface is more positively charged at lower pH from protonation. At the protonated sites, adsorbed water molecules prefer to bind with their O connected to the surface. In addition, the increasing surface field created by the surface charges also tends to reorient more water molecules with O facing the surface, some of which have ice-like tetrahedral bonding with neighbors and contribute to the negative-amplitude ice-like band in the spectrum. Increasing the pH from 7.5 creates an opposite situation. The alumina surface becomes more deprotonated and negatively charged. Water molecules prefer to be H-bonded with their H attached to the depronated sites and the surface field tends to reorient water molecules with H facing the surface. Both mechanisms contribute positively to the amplitudes of the ice-like and liquid-like bands. Therefore, increasing pH makes the initially negative amplitude of the liquid-like band less negative, and the initial weak amplitude of the ice-like band more positive. We note in passing that the dangling OH cannot experience the surface field and hence the surface field effect, but deprotonation does reduce their surface density and therefore their intensity, as seen in Figure 3 with pH > 8.2.

We now return to the discussion of p.z.c.. Previous second harmonic generation (SHG) and streaming potential measurements found that the p.z.c. for α-Al_2O_3 (0001) appeared between pH 4-6,[16,17,21,22] which overlaps with the value 6.3±1.2 we have obtained. All of these values are significantly smaller than the p.z.c. found for powder alumina which is pH 8-10.[13] The difference is believed to arise from the different bonding environments of surface Al_nOH groups in powder samples and crystalline samples.[17,52] We describe here how one can understand the p.z.c. of a particular surface if the pK values of protonation and deprotonation of the surface are known. Schwarz et al.[19] pointed out that different surface sites on alumina could have drastically different charging behaviors depending on the acidity of the surface Al_nOH groups. Using potentiometric titration, they measured four distinct pKs (pK= -logK) for reactions of surface Al_nOH groups, which are: $pK_1 \leq 3$, $pK_2=4.5$, $pK_3=6.7$, and $pK_4=9.7$.[19] Although

assignment of these pK values to specific protonation/deprotonation reactions is not definitive, a general trend has been proposed by Schwarz[19] and Eisenthal[22] based on partial charges of the Al_nOH groups, as we shall discuss here.

From Pauling's bond valence rule, the net bond valence on the oxygen of the $(Al)_nOH$ species are: +0.5 for $(Al)_3OH$, 0 for $(Al)_2OH$, and –0.5 for (Al)OH.[19] Here, all Al atoms are assumed to be octahedrally bonded to neighbors as in the bulk, and thus each Al atom donates 3/6=0.5 bond valence to the oxygen while the proton donates +1 to the oxygen if it is not involved in hydrogen bonding. As the bond valence on the hydroxyl oxygen atom decreases for $(Al)_nOH$ with n changes from 3 to 1, we infer that the O-H bond is stronger and the OH becomes more difficult to deprotonate. The acidity of the OH group therefore has the following trend: $(Al)_3OH > (Al)_2OH > (Al)OH$.[19] Based on this knowledge of acidity, we assign the pK values listed in Ref. 19 to the following chemical reactions for different Al_nOH species:

$$(Al)OH^{-0.5} \leftrightarrow (Al)O^{-1.5} + H^+ \qquad pK \sim 13 \qquad (7)$$

$$(Al)_2OH^0 \leftrightarrow (Al)_2O^- + H^+ \qquad pK = 9.7 \qquad (8)$$

$$(Al)_3OH^{+0.5} \leftrightarrow (Al)_3O^{-0.5} + H^+ \qquad pK = 6.7 \qquad (9)$$

$$(Al)OH_2^{+0.5} \leftrightarrow (Al)OH^{-0.5} + H^+ \qquad pK = 4.5 \qquad (10)$$

$$(Al)_2OH_2^+ \leftrightarrow (Al)_2OH^0 + H^+ \qquad pK \le 3 \qquad (11)$$

On α-Al_2O_3 (0001), the surface hydroxyl groups are $(Al)_2OH$. The protonation and deprotonation reactions are described by Eqs. (11) and (8), respectively. This agrees well with our SFVS observation in Figs. 3 and 6 that at pH 3.3 and 9.3, the alumina surface is already significantly protonated and deprotonated, respectively. From the pK values of reactions (8) and (11) for protonation and deprotonation of $(Al)_2OH$, we can find the p.z.c.. For deprotonation and protonation, the equilibrium conditions are

$$K_8=[Al_2O^-][H^+]/[Al_2OH] \qquad (12)$$

$$K_{11}=[Al_2OH][H^+]/[Al_2OH_2^+] \qquad (13)$$

At the p.z.c., we should have $[Al_2O^-]=[Al_2OH_2^+]$, and therefore $[H^+]^2=K_8K_{11}$ or $pH=(pK_8+pK_{11})/2$. With pK_8 = 9.7 and pK_{11} = 3, we find pK = 6.35, which is very close to what we deduced from the SFVS result.

In previous interfacial studies, the pH value at which dissolution of salt has no effect on the interfacial structure, known as the point of zero salt effect (p.z.s.e), was often used to find p.z.c.,[21,22,53] because in the absence of surface charges, salt ions are not attracted to the interface. In our SFVS study, this means that at the p.z.c., addition of salt into the aqueous solution should not change the spectrum. Figure 8 displays SFVS spectra of water/α-Al_2O_3 (0001) interfaces with and without salt at three different pH values: below, near, and above p.z.c.. When the pH is far from p.z.c., the signal intensity with 50mM NaCl is much weaker than that without NaCl. Screening of the surface field by the electrolyte in the double charge layer is the main reason for reduction of the SF signal from the interfacial water. At pH 5.8, the spectrum is essentially the same with and without NaCl. The p.z.s.e. is therefore near pH 6, which agrees well with our estimated p.z.c. at pH 6.3 described earlier.

We can now qualitatively understand the difference of p.z.c. between α-Al_2O_3 (0001) and powder α-Al_2O_3. The α-Al_2O_3 particles in the powder sample have many exposed crystalline planes with different surface sites including many edge sites. We expect an increased number of OH groups bonded to just one Al atom with unsaturated bonding at the surfaces. The corresponding deprotonation reaction (7) with pK > 10 and the protonation reaction (10) with pK =4.5 may play an important role in determining the overall charging condition on the particles and hence increase the p.z.c. closer to the reported value of pH 8-10.[13,24-26]

In a recent study by Kershner et al,[16] it was shown that crystalline alumina powder with relatively uniform shapes (Sumitomo AA-2) has p.z.c. at pH 3.8, while random-shaped alumina powder (Sumitomo AKP-30) has p.z.c. around pH 8. They suggested that the large difference lies in the surface structures of the particles. The AA-2 particles had well-defined surface facets that resembled a calculated Wulff shape[54] with R-plane as the dominant surface. On the other hand, the AKP-30 particles did not have a specific dominant crystalline plane. Franks and Gan recently reported a similar finding.[52]

They found that α-Al_2O_3 platelets with mainly (0001) surfaces had a p.z.c. around pH 4-7, and AKP-50 "potato-shaped" alumina particles showed a p.z.c. around pH 9.5. According to Franks and Meagher,[17] surfaces of alumina powder particles might be terminated in such a haphazard way that it is almost like the surface of amorphous alumina. Measuring the p.z.c. of amorphous alumina can provide support to this postulation.

Figure 9 shows the spectra from an amorphous Al_2O_3/water interface at different pH and the plot of spectral intensity at 3200 cm^{-1} versus pH (Figure 9(f)). The p.z.c. of the surface corresponding roughly to the minimum intensity in the plot is near pH 9.7, similar to that of alumina powder. This suggests that the amorphous surface may indeed have an average surface structure (at least in terms of $(Al)_nO$ coordination) similar to that of alumina powder with (Al)OH as dominant species on the surface.

Conclusions

We have used SFVS to study structure and charging behavior of water/α-Al_2O_3 (0001) interfaces. The SF vibrational spectrum in the OH stretch region exhibits, in general, three spectral features similar to those of other water interfaces: a prominent peak at 3700 cm^{-1}, a liquid-like band at 3450 cm^{-1}, and an ice-like band at 3200 cm^{-1}, indicating that the water interfacial structure is a highly distorted H-bonding network. The 3700 cm^{-1} peak can be attributed to the protruding OH associated with Al_2OH groups on the bulk-terminated α-Al_2O_3 (0001) surface. It already exists at the air/α-Al_2O_3 (0001) surface, and persists when the surface is immersed in water, but its strength decreases when the bulk pH is sufficiently large (> 8.2) to appreciably deprotonate these surface Al_2OH groups.

The liquid-like band comes from water molecules H-bonded to the alumina surface as well as those underneath with asymmetric bonding to the neighbors. The ice-like peak comes from water molecules with symmetric tetrahedral bonding to the neighbors. Their strengths vary with pH. While water species contributing to the liquid-like band always have a net polar orientation with OH pointing toward the liquid, those contributing to the ice-like band have the net polar orientation switched in the mid pH range. The variations with pH can be understood as results of protonation and deprotonation of the

surface Al_2OH groups that leave the surface positively and negatively charged, respectively, depending on pH. Protonation or deprotonation alters the average polar orientations of water molecules H-bonded to the alumina surface and also creates a surface field that reorients the interfacial water molecules not directly bonded to the surface.

The spectral variation of the ice-like band, including the sign change of its amplitude, allows us to determine the p.z.c. of α-Al_2O_3 (0001) to be around pH 6.3. It agrees with an estimate based on the reaction rates of the protonation and deprotonation processes at the water/α-Al_2O_3 (0001) interface. It also agrees within uncertainty with values determined by others in earlier studies.[55] This p.z.c. value is significantly lower than that of powder alumina and amorphous alumina. The difference is believed to be due to existence of multiple forms of Al_nOH groups at the surfaces of powder alumina particles and amorphous alumina.

We plan to extend such investigation to interfaces of water with other crystalline alumina surfaces. The SFVS technique described here to study the water/α-Al_2O_3 (0001) interface and its charging behavior with pH can also be applied to studies of other liquid/oxide interfaces.

Acknowledgment. This work was supported by the NSF Science and Technology Center of Advanced Materials for Purification of Water with Systems (Water CAMPWS; CTS-0120978). We also acknowledge support from the Director, Office of Science, Office of Basic Energy Sciences, Materials Sciences and Engineering Division as well as the Chemical Sciences, Geosciences, and Biosciences Division, of the U.S. Department of Energy under contract No. DE-AC02-05CH11231.

References and Notes

(1) Brown, G. E. Jr; Henrich, V. E.; Casey, W. H.; Clark, D. L.; Eggleston, C.; Felmy, A.; Goodman, D. W.; Gratzel, M.; Maciel, G.; McCarthy, M. I.; Nealson, K. H.; Sverjensky, D. A.; Toney, M. F.; Zachara, J. M. Chem. Rev 1999, 99, 77-174.

(2) Lefevre, G. Advances in Colloid and Interface Science, 2004, 107, 109-123.

(3) Al-Abadleh, H. A.; Grassian, V. H. Surface Science Reports, 2003, 52, 63-161.

(4) Rietra, R. R. J. J.; Hiemstra, T.; van Riemsdijk, W. H. Geochim. Cosmochim. Acta 1999, 63, 3009-3015.

(5) Behrens, S. H.; Borkovec, M. J. Phys. Chem. B 1999, 103, 2918-2928.

(6) Sormorjai, G. A. Introduction to Surface Chemistry and Catalysis, Wiley, New York, 1994.

(7) Zhang, H. Z.; Gilbert, B.; Huang, F.; Banfield, J. F. Nature, 2003, 424, 1025-1029.

(8) Kurnosikov, O.; Pham Van, L.; Cousty, J. Surf. Sci. 2000, 459, 256-264.

(9) Gan, Y.; Franks, G. V. J. Phys. Chem. B 2005, 109, 12474-12479.

(10) Trainor, T. P.; Fitts, J. P.; Templeton, A. S.; Grolimund, D.; Brown, G. E. J. Colloid Interface Sci. 2001, 244, 239-244.

(11) Templeton, A. S.; Trainor, T. P.; Traina, S. J.; Spormann, A. M.; Brown, G. E. Proc. Natl. Acad. Sci. U.S.A. 2001, 98, 11897-11902.

(12) Eng, P. J.; Trainor, T. P.; Brown, G. E.; Waychunas, G. A.; Newville, M.; Sutton, S. R.; Rivers, M. L. Science 2000, 288, 1029-1033.

(13) Kosmulski, M. Chemical Properties of Material Surfaces, Marcel Dekker, Inc. New York, 2001.

(14) Modi, H. J.; Fuerstenau, D. W. J. Phys. Chem. 1957, 61, 640-643.

(15) O'Connor, D. J.; Johansen, P. G.; Buchanan, A. S. Trans. Faraday Soc. 1956, 52, 229-236.

(16) Kershner, R. J.; Bullard, J. W.; Cima, M. J. Langmuir 2004, 20, 4101-4108.

(17) Franks, G. V.; Meagher L. Colloids Surf. Sci. A: Physicochem Eng. Aspects 2003, 214, 99-110.

(18) Valdivieso, A. L.; Bahena, J. L. R.; Song, S.; Urbina, R. H. J. Colloid Inter. Sci. 2006, 298, 1-5.

(19) Contescu, C.; Jagiello, J.; Schwarz, J. A. Langmuir 1993, 9, 1754-1765.

(20) Veeramasuneni, S.; Yalamanchili, M. R.; Miller, J. D. J. Colloid Inter. Sci. 1996, 184, 594-600.

(21) Stack, A. G.; Higgins, S. R.; Eggleston, C. M. Geochimica et Cosmochimica Acta, 2001, 65, 3055-3063.

(22) Fitts, J. P.; Shang, X. M.; Flynn, G. W.; Heinz, T. F.; Eisenthal, K. B. J. Phys. Chem. B 2005, 109, 7981-7986.

(23) Yeganeh, M. S.; Dougal, S. M.; Pink, H. S. Phys. Rev. Lett. 1999, 83, 1179-1182.

(24) Kosmulski, M. J. Coll. Int. Sci. 2006, 298, 730-741.

(25) Kosmulski, M. J. Coll. Int. Sci. 2004, 275, 214-224.

(26) Kosmulski, M. J. Coll. Int. Sci. 2002, 253, 77-87.

(27) Ostroverkhov, V.; Waychunas, G. A.; Shen, Y. R. Chem. Phys. Lett. 2004, 386, 144-148.

(28) Ostroverkhov, V.; Waychunas, G. A.; Shen, Y. R. Phys. Rev. Lett. 2005, 94, 046102.

(29) Schrodle, S.; Richmond, G. L. J. Phys. D-Appl. Phys. 2008, 41, 033001.

(30) Shen, Y. R.; Ostroverkhov, V. Chemical Reviews, 2006, 106, 1140-1154.

(31) Somorjai, G. A.; Park, J. Y. Physics Today, 2007, 60, 48-53.

(32) Shen, Y. R. In Frontiers in Laser Spectroscopy, *Proceedings of the International School of Physics* 'Enrico Fermi'; Hansch, T. W.; Inguscio, M., Eds.; Course CXX, North-Holland: Amsterdam, 1994; p 139-165.

(33) Miranda, P. B.; Shen, Y. R. J. Phys. Chem. B 1999, 103, 3292-3307.

(34) Chen, Z.; Shen, Y. R.; Somorjai, G. A. Annu. Rev. Phys. Chem. 2002, 53, 437-465.

(35) Smith, J. D.; Cappa, C. D.; Wilson, K. R.; Cohen, R. C.; Geissler, P. L.; Saykally, R. J. Proc. Natl. Acad. Sci. USA 2005, 102, 14171-14174.

(36) Eaves, J. D.; Loparo, J. J.; Fecko, C. J.; Roberts, S. T.; Tokmakoff, A.; Geissler, P. L. Proc. Natl. Acad. Sci. USA 2005, 102, 13019-13022.

(37) Levine, B. F.; Bethea, C. G. J. Chem. Phys. 1976, 65, 2429-2438.

(38) Kielich, S. IEEE J. Quantum Electron. QE 5 1969, 562.

(39) Ong, S.; Zhao, X.; Eisenthal, K. B. Chem. Phys. Lett. 1992, 191, 327-334.

(40) Ott, A. W.; McCarley, K. C.; Klaus, J. W.; Way, J. D.; George, S. M. Appl. Surf. Sci. 1996, 107, 128-136.

(41) Ji, N.; Ostroverkhov, V.; Chen, C. Y.; Shen, Y. R. J. Am. Chem. Soc. 2007, 129, 10056.

(42) Al-Abadleh, H. A.; Grassian, V. H. Langmuir 2003, 19, 341-347.

(43) Hass, K. C.; Schneider, W. F.; Curioni, A.; Andreoni, W. Science, 1998, 282, 265-268.

(44) Morterra, C.; Magnacca, G. Catalysis Today 1996, 27, 497-532.

(45) Tsyganenko, A. A.; Mardilovich, R. R. J. Chem. Soc., Faraday Trans.1996, 92, 4843-4852.

(46) Peri, J. B. J. Phys. Chem. 1965, 69, 220-230.

(47) Chen, J. G.; Crowell, J. E.; Yates, J. T. J. Chem. Phys. 1986, 84, 5906-5909.

(48) Coustet, V.; Jupille, J. Surf. Sci. 1994, 307, 1161-1165.

(49) Guo, J.; Ellis, D. E.; Lam, D. J. Phys. Rev. B 1992, 45, 13647-13656.

(50) Du, Q.; Freysz, E.; Shen, Y. R. Phys. Rev. Lett. 1994, 72, 238-241.

(51) Duval, Y.; Mielczarski, J. A.; Pokrovsky, O. S.; Mielczarski, E.; Ehrhardt, J. J. J. Phys. Chem. B 2002, 106, 2937-2945.

(52) Franks, G. V.; Gan, Y. J. Am. Ceram. Soc. 2007, 90, 3373-3388.

(53) Sposito, G. Environ. Sci. Technol. 1998, 32, 2815-2819.

(54) Kitayama, M.; Powers, J. D.; Kulinsky, L.; Glaeser, A. M. J. Eur. Ceram. Soc. 1999, 19, 2191-2209.

(55) After submission of our paper, the following reference appeared. Braunschweig, B.; Eissner, S.; Daum, W. J. Phys. Chem. C. 2008, 112, 1751. The work also focused on SFVS spectra of water/α-Al_2O_3(0001) interfaces at different pH, but their sample preparation method was different from ours, leading to some differences in the spectra. The very thin sample (0.5 mm) they used could be a problem if interference of beams from the two surfaces had to be avoided. We thank the reviewer for bringing the following conference abstracts on SFVS studies of water/alumina interfaces to our attention: Florsheimer, M. et al., Geochimica et Cosmochimica Acta 2007, 71, A286; Florsheimer, M. et al., ibid, 2005, 69, A484; Florshiemer, M. et al, ibid, 2004, 68, A120. While part of their stated results are in agreement with ours, their observation of as many as 7-9 peaks in the spectra suggests that their sample surface was quite different from ours.

Figure captions:

Figure 1

SSP sum-frequency vibrational spectra of the following interfaces: (a) α-Al_2O_3 (0001)/air after cleaning; (b) α-Al_2O_3 (0001)/H_2O (solid square), α-Al_2O_3 (0001)/D_2O (open triangle), and α-Al_2O_3 (0001)/air (open circle) after retrieving from D_2O; (c) α-Al_2O_3 (0001)/air after heating at 600C for 1 hour (solid triangle), and then after being exposed to ambient air for 48 hours (open square). Solid lines on the spectra are fits using Eq. (2) with three discrete resonances.

Figure 2

Sum-frequency vibrational spectra of the α-Al_2O_3 (0001)/air interface with SSP, PPP, SPS polarization combinations. The solid curves are fits using Eq. (2).

Figure 3

SSP sum-frequency vibrational spectra of α-Al_2O_3 (0001)/water interface at different bulk pH. Solid lines on the spectra are fits using Eq. (2) with three discrete resonances.

Figure 4

Sum-frequency vibrational spectra of α-Al_2O_3 (0001)/water interfaces with SSP, PPP, SPS polarization combinations at three different pH. (a) pH=3.3; (b) pH=5.8, and (c) pH=9.8.

Figure 5

Spectra of $|\chi_{eff}|^2$ and $Im\chi_{eff}$ of α-Al_2O_3 (0001)/water interfaces with SSP polarization combination. (a) Intensity spectra showing $|\chi_{eff}|^2$ at pH=3.3; (b) Measured $Im\chi_{eff}$ (open circles) and fitting results of (a) using Eq.(2); (c) Intensity spectra showing $|\chi_{eff}|^2$ at pH=9.0; (d) Measured $Im\chi_{eff}$ (open squares) and fitting results of (c) using Eq.(2). The pH 3.3 and pH 9.0 values are below and above p.z.c., respectively.

Figure 6

Amplitudes of the ice-like and liquid-like bands, deduced from fitting of the spectra in Figure 3 with Eq.(2), versus pH.

Figure 7

Schematic showing the side view along (11-20) of the structure of a bulk-terminated fully hydroxylated α-Al_2O_3 (0001) surface covered by Al_2-OH groups. Aluminum atoms are colored purple, oxygen atoms red, and hydrogen atoms gray.

Figure 8

Sum-frequency vibrational spectra of the α-Al_2O_3(0001)/water interface at three different pH. (a) pH=3.3; (b) pH=5.8, and (c) pH=9.8. In each panel, the upper spectrum is for aqueous solution without NaCl, and the bottom spectrum is with 50mM of NaCl.

Figure 9

(a)-(e) SSP sum-frequency vibrational spectra of an amorphous alumina/water interface with different pH. (f) Plot of $|\chi_{eff}|^2$ versus pH. The point of zero charge occurs around pH 9.7.

TABLE OF CONTENS GRAPHIC

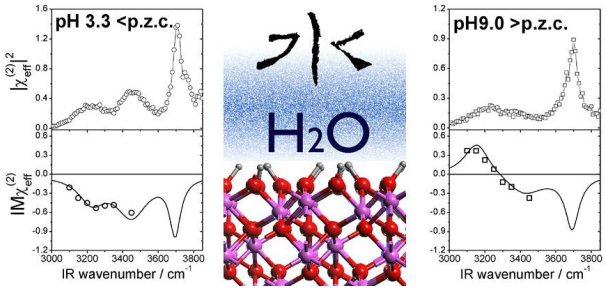

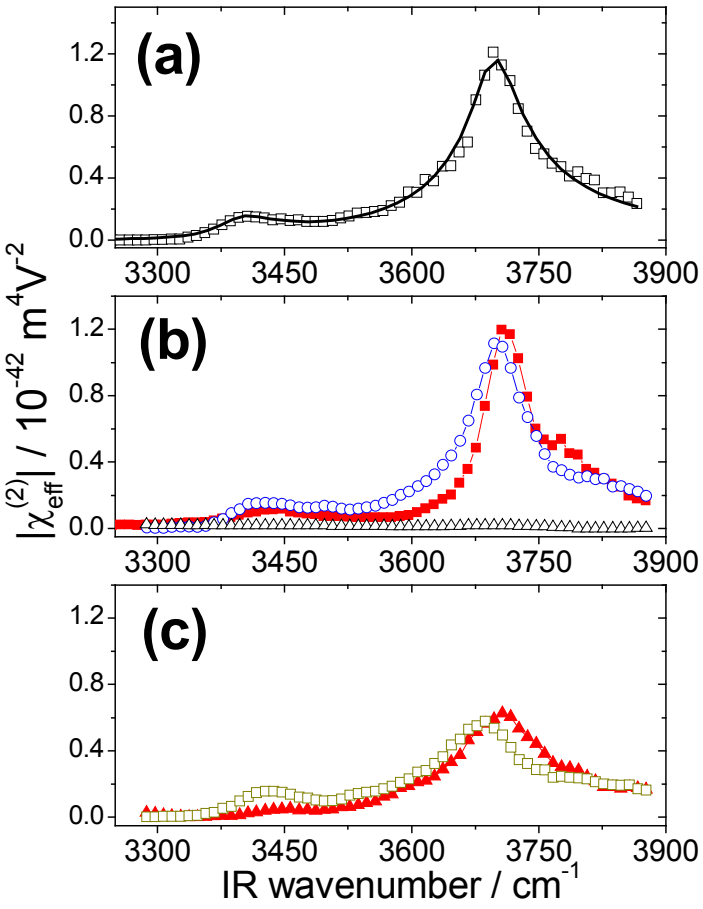
(a)
(b)
(c)
1.2
0.8
0.4
0.0
3300
3450
3600
3750
3900
$|\chi^{(2)}_{eff}|$ / 10^{-42} m^4V^{-2}
IR wavenumber / cm^{-1}

Figure 1

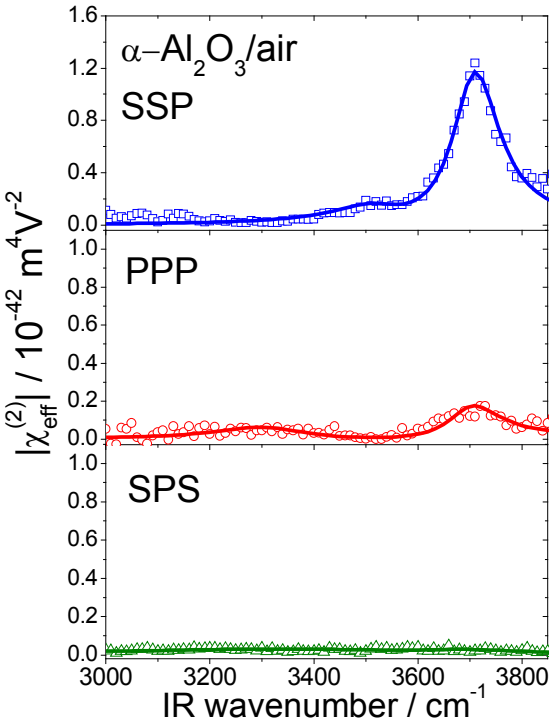
α–Al2O3/air
SSP
PPP
SPS
|χ(2)eff| / 10-42 m4V-2
IR wavenumber / cm-1
1.6
1.2
0.8
0.4
0.0
1.0
0.6
0.2
3000
3200
3400
3600
3800

Figure 2

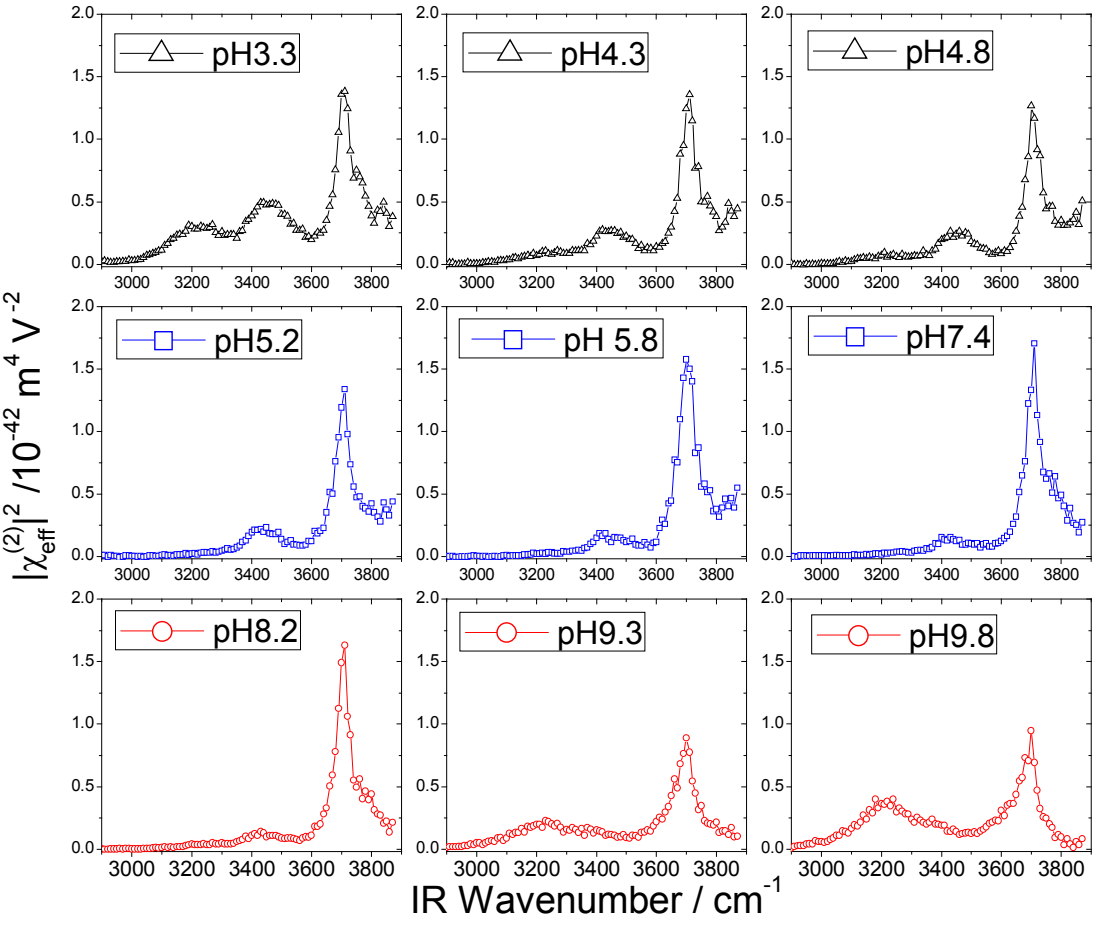
pH3.3
pH4.3
pH4.8
pH5.2
pH 5.8
pH7.4
pH8.2
pH9.3
pH9.8
$|\chi^{(2)}_{eff}|^2$ /10^{-42} m^4 V^{-2}
IR Wavenumber / cm^{-1}

Figure 3

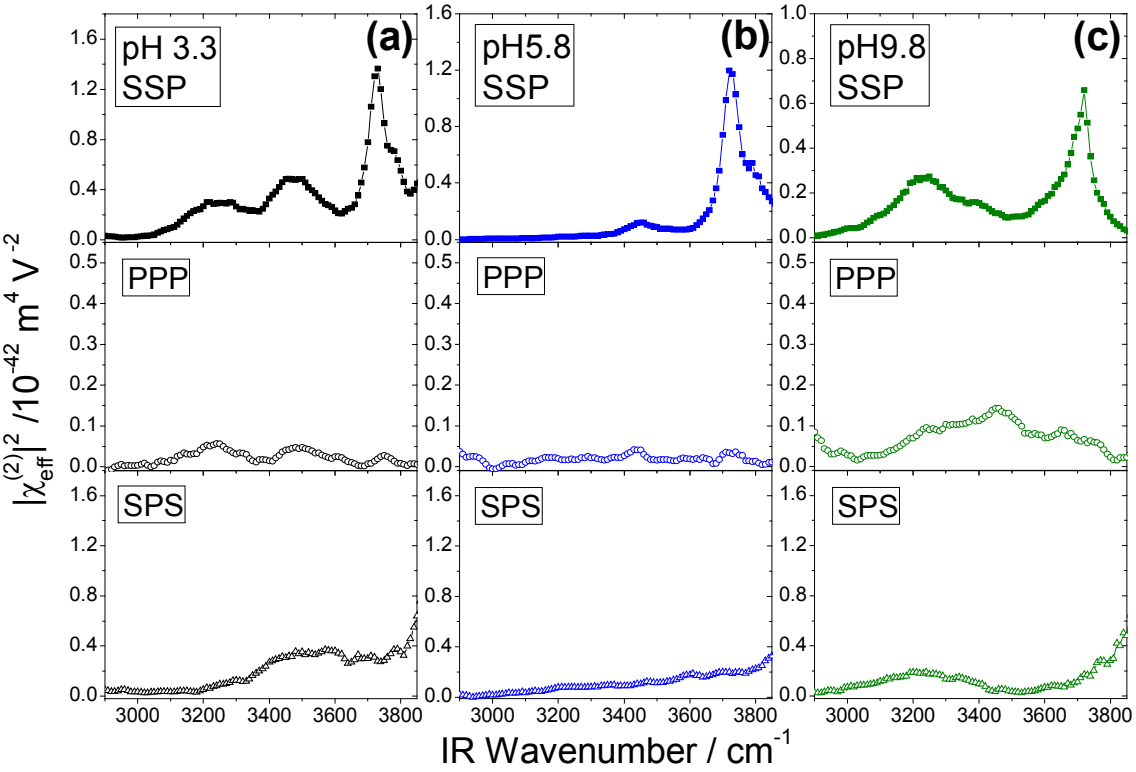
pH 3.3
SSP
(a)
pH5.8
SSP
(b)
pH9.8
SSP
(c)
PPP
PPP
PPP
SPS
SPS
SPS
$|\chi^{(2)}_{eff}|^2$ /10^{-42} m^4 V^{-2}
IR Wavenumber / cm^{-1}

Figure 4

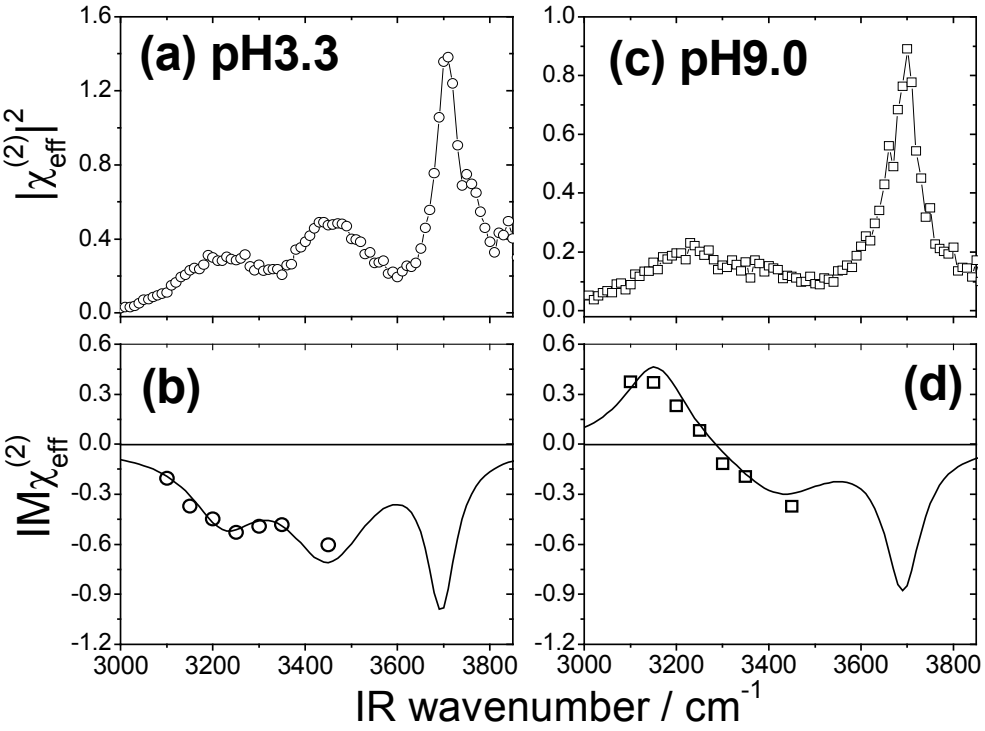

Figure 5

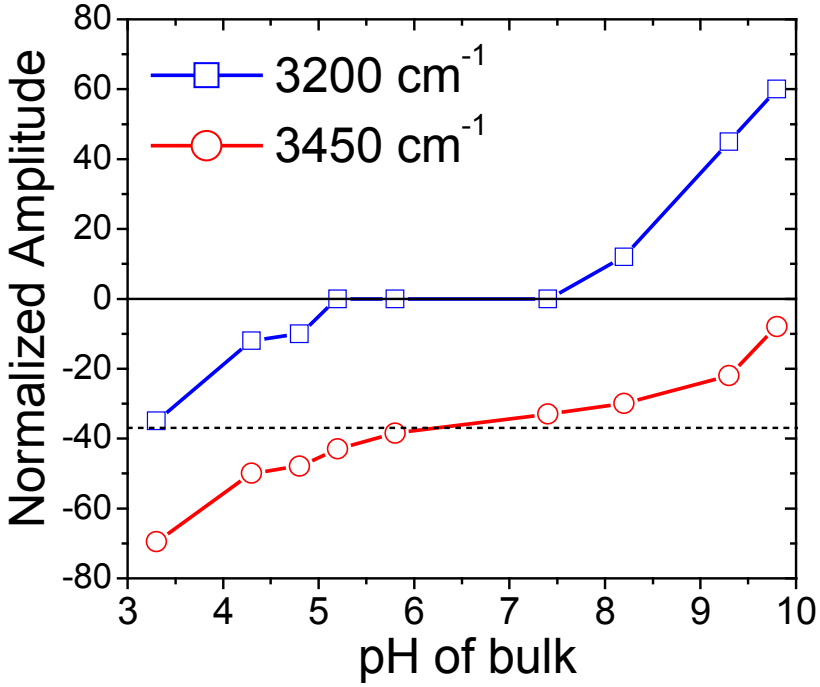
3200 cm-1
3450 cm-1
Normalized Amplitude
pH of bulk
80
60
40
20
0
-20
-40
-60
-80
3
4
5
6
7
8
9
10

Figure 6

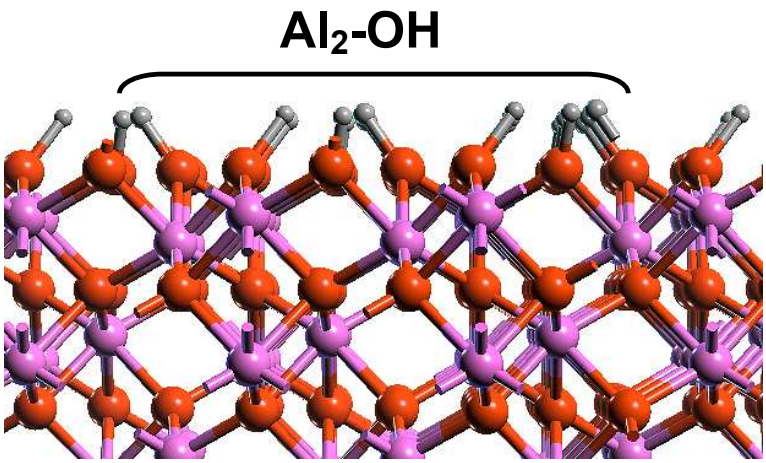

Figure 7

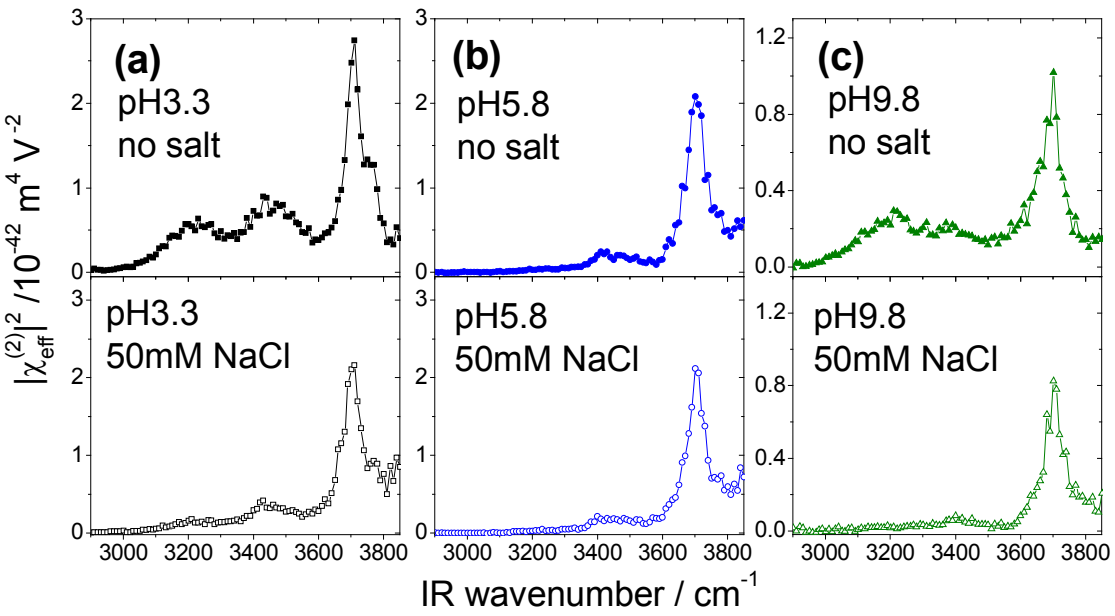
(a)
pH3.3
no salt
(b)
pH5.8
no salt
(c)
pH9.8
no salt
pH3.3
50mM NaCl
pH5.8
50mM NaCl
pH9.8
50mM NaCl
$|\chi^{(2)}_{eff}|^2$ /10^{-42} m^4 V^{-2}
IR wavenumber / cm^{-1}

Figure 8

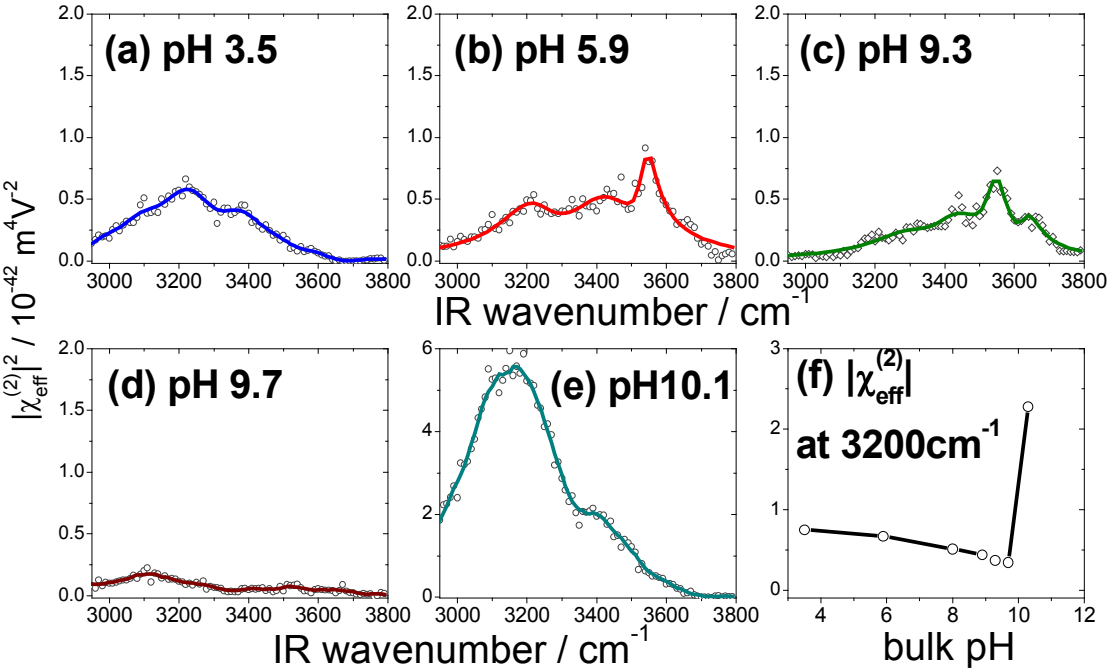
(a) pH 3.5
(b) pH 5.9
(c) pH 9.3
(d) pH 9.7
(e) pH10.1
(f) |χ(2)eff|
at 3200cm-1
|χ(2)eff|2 / 10-42 m4V-2
IR wavenumber / cm-1
IR wavenumber / cm-1
bulk pH

Figure 9